Multistimuli Responsive Supramolecular Vesicles Based on the Recognition of *p*-Sulfonatocalixarene and its Controllable Release of Doxorubicin

Kui Wang, Dong-Sheng Guo, Xiang Wang, and Yu Liu*

Department of Chemistry, State Key Laboratory of Elemento-Organic Chemistry, Nankai University, Tianjin 300071, P. R. China

ABSTRACT We report the novel construction of nanosupramolecular binary vesicles based on host–guest complex formation between *p*-sulfonatocalix[4]arene and asymmetric viologen, which was identified by UV–vis and fluorescence spectroscopy, dynamic laser scattering, transmission electron microscopy, scanning electron microscopy, and surface tension experiments. The critical aggregation concentration of asymmetric viologen decreases pronouncedly by a factor of *ca.* 1000 owing to the complexation of *p*-sulfonatocalix[4]arene. Furthermore, we have demonstrated that the resulting vesicles can respond to multiple external stimuli, including temperature, host–guest inclusion, and redox. Methods of warming and inclusion of cyclodextrins were then employed to disrupt the vesicle architecture to release hydrophilic doxorubicin from the interior of the vesicle. Finally, cell experiments were performed to evaluate the cellular toxicity of the supramolecular binary vesicle and the anticancer efficiency of doxorubicin-loaded vesicle.

KEYWORDS: multistimuli responsive · vesicles · calixarenes · host–guest systems · aggregation

Vesicles are ubiquitous building blocks in living systems and are significantly useful in the fields of chemistry, biology, and material science. Construction of vesicles with desired shape, size, and properties endow them special functions for the development of biomimetic systems, drug/gene delivery systems, light-harvesting systems, and microreactors.[1–12] Controllable switching assembly on/off is a prerequisite to achieve potential applications.[13–19] Consequently, studies on stimuli–response of vesicles have become an extraordinarily fascinating topic. Grafting stimuli–responsive sites onto building blocks can lead to the fabrication of smart vesicle systems that are responsive to photo-, electro-, thermo-, pH-, or chemo-stimuli.[16,20–32] However, to the best of our knowledge, all the stimuli–responsive vesicles reported only deal with response to single stimulus up to now, although there have been a few reports about multistimuli responsive polymeric micelles and gels.[33–37] In nature, the change in behavior of a macromolecule, such as proteins and nucleic acids, is often a result of its response not to a single factor, but to a combination of environmental changes.[33] To mimic this feature, construction of materials which can respond to multiple stimuli in a predictable manner would be of great interest.[33–38]

Besides the irreversible covalent route, the supramolecular approach paves an alternative way to build micelles, vesicles, and other amphiphilic assemblies. Because such assemblies are held together by multiple weak and therefore reversible interactions, supramolecular amphiphiles are a particularly responsive and tunable form of soft matter.[34,39] Until now, several kinds of noncovalent interactions have been used to fabricate supramolecular amphiphiles, including hydrogen-bonding, charge-transfer, and $\pi\cdots\pi$ interactions, among others.[40–51] However, supramolecular vesicles based on host–guest interactions have been explored much less frequently.[29,52–54] The host–guest complexation events based on cyclodextrin, sulfonatocalixarene, and cucurbituril macrocycles occur commonly in aqueous media, where some other noncovalent interactions are not always effective.[55] Moreover, such macrocycles have been demonstrated to be significantly biocompatible.[56–61] Construction of supramolecular vesicles from these macrocycles is of fundamental interest for applications in biotechnology and medicine.

In this work, we report the successful construction of multistimuli-responsive nanosupramolecular binary vesicles from water-soluble calixarene and asymmetric viologen, driven by host–guest complexation. In fact, there have been certain reports on amphiphilic assemblies

* Address correspondence to yuliu@nankai.edu.cn.

Received for review December 15, 2010 and accepted March 28, 2011.

Published online March 28, 2011
10.1021/nn1034873

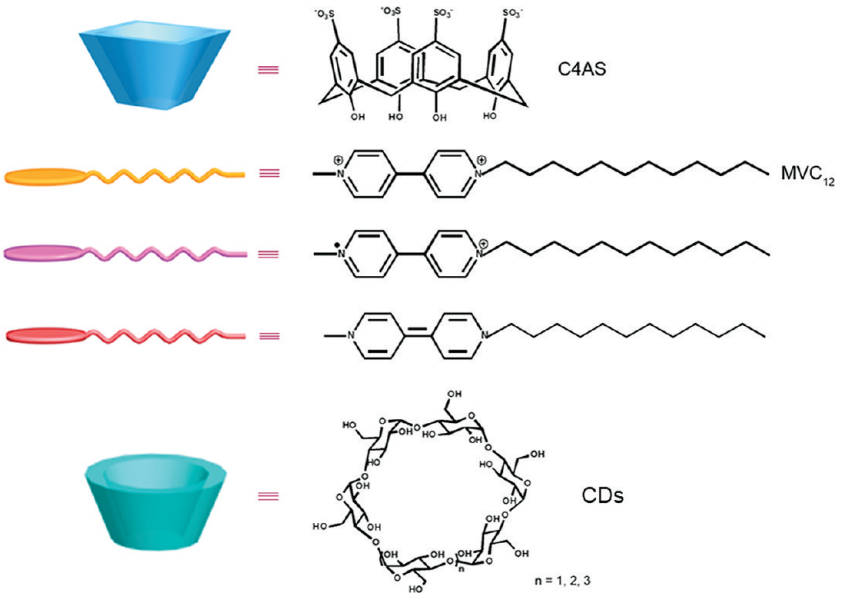

Scheme 1. Structural illustration of *p*-sulfonatocalix[4]arene (C4AS), asymmetric viologen (MVC_{12}), and cyclodextrins (CDs).

based on calixarenes.[16,62−67] Their intrinsic cone shape is the prerequisite for high-curvature aggregations of amphiphiles, and their relatively rigid framework can enhance the aggregation stability.[16,62,68] All these examples are uniformly built up *via* a covalent approach that modifies calixarenes into amphiphiles by the linkage of lipophilic groups at one rim and hydrophilic groups at the other rim, where calixarenes act as simple scaffolds only. The cavity encapsulation of calixarenes is almost neglected except for two recent examples by our group and others.[69,70] In the previous work, we reported the construction of a supramolecular binary vesicle upon complexation of *p*-sulfonatocalix[5]arene with 1-pyrenemethylaminium guest, where the calix cavity was first exploited. As a part of our ongoing program concerning the supramolecular vesicles based on water-soluble calixarene macrocycles, a new nanosupramolecular binary vesicle was fabricated here from *p*-sulfonatocalix[4]arene (C4AS) and 1-methyl-1′-dodecyl-4,4′-bipyridinium (MVC_{12}) (Scheme 1). The complexation of C4AS with organic guests is dominantly enthalpy-driven and would be weakened upon warming. The molecular amphiphilicity of MVC_{12} can be tuned by either redox or inclusion of cyclodextrins (CDs). Therefore, the present system is reasonably anticipated to show fascinating multistimuli responses.

RESULTS AND DISCUSSION

Construction of Supramolecular Binary Vesicles Based on the Host−Guest Complexation of C4AS with MVC_{12}. The critical aggregation concentrations (CAC) of MVC_{12} in the presence of C4AS were measured by monitoring the dependence of the absorbance at 450 nm on the concentration of MVC_{12}.[71−73] In the absence of C4AS, the maximum absorption of MVC_{12} at 260 nm increases linearly versus its increasing concentrations from 0.01 to 0.10 mM, and no absorption band is observed at longer wavelengths (Supporting Information, Figure S1a). Besides that, the quenching of the excited pyrene probe molecules proceeds so slowly at diffusion-controlled rates (Supporting Information, Figure S1b). These two results indicate that MVC_{12} cannot aggregate in this concentration range, coinciding with the CAC value (*ca.* 2×10^{-2} M) of MVC_{12} reported before.[71] In the presence of C4AS, a broad absorption appears at longer wavelengths (Figure 1a), belongs to the charge−transfer complexation of calixarene with viologen and $\pi\cdots\pi$ aggregation of viologen themselves. The complexation-induced CAC can therefore be obtained according to the plot of absorbance at 450 nm *versus* concentration of MVC_{12}: 0.02 mM at 0.02 mM C4AS, 0.04 mM at 0.05 mM C4AS, and 0.07 mM at 0.08 mM C4AS (Figure 1b−d). Excitingly, the CAC value of MVC_{12} decreases pronouncedly by a factor of *ca.* 1000 due to the complexation of C4AS. Fluorescence spectra of the solutions containing pyrene probe molecules show that in the presence of C4AS the relative fluorescence intensity of pyrene diminishes dramatically with the increasing MVC_{12} concentration (Figure 2 and Supporting Information, Figure S2). The efficient quenching can be explained by the proximity of the pyrene molecules to the viologen headgroup if one accepts the increasingly widespread view that nonpolar molecules like pyrene are solubilized near the Stern layer in ionic micelles,[74] which also proves the formation of amphiphilic aggregation. It is noted that C4AS is without any tendency to self-aggregation in aqueous solution.[75] Control experiments show that replacement of C4AS by its building subunit 4-phenolsulfonic sodium could not induce the formation of aggregation (Figure 3 and Supporting Information, Figure S3), indicating undoubtedly the host−guest complexation of C4AS is the crucial factor leading to MVC_{12} aggregation, where

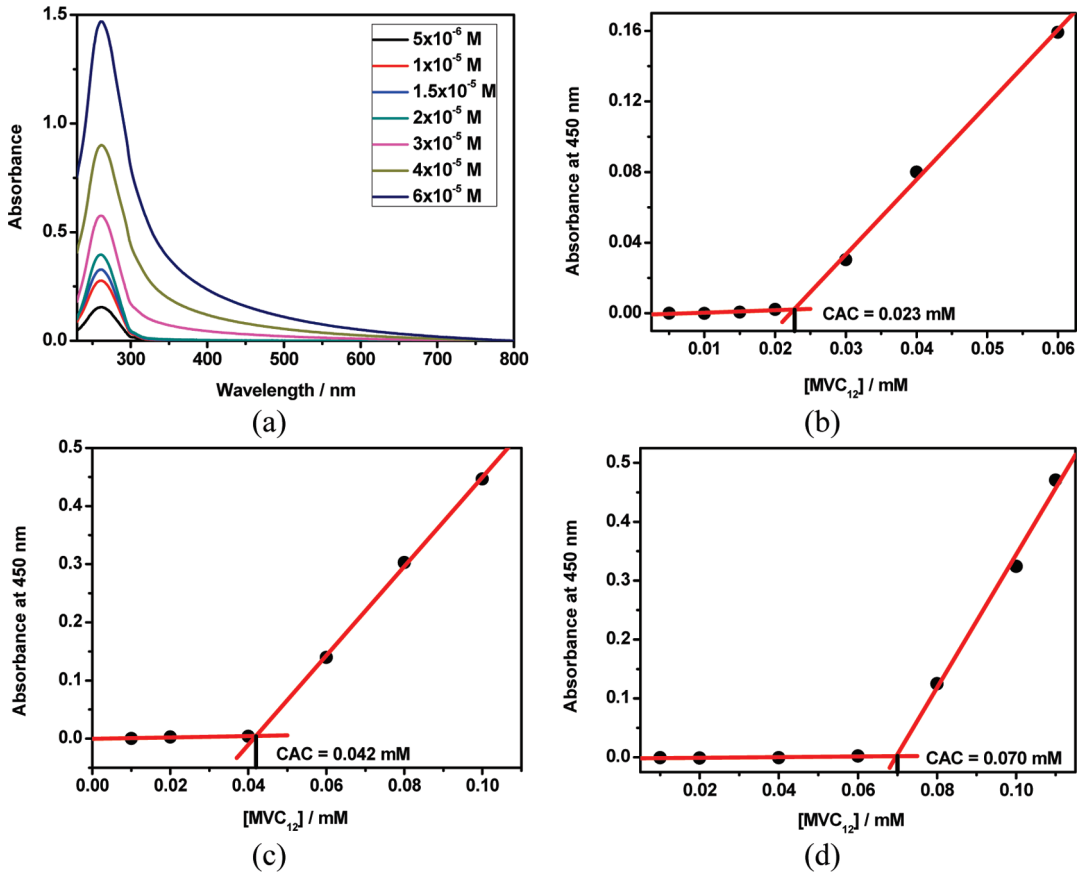

Figure 1. (a) UV−vis absorption spectra of aqueous solutions of MVC_{12} at different concentrations in the presence of 0.02 mM C4AS at 25 °C. Dependence of the absorbance at 450 nm on MVC_{12} concentration in the presence of C4AS: 0.02 mM (b), 0.05 mM (c), 0.08 mM (d).

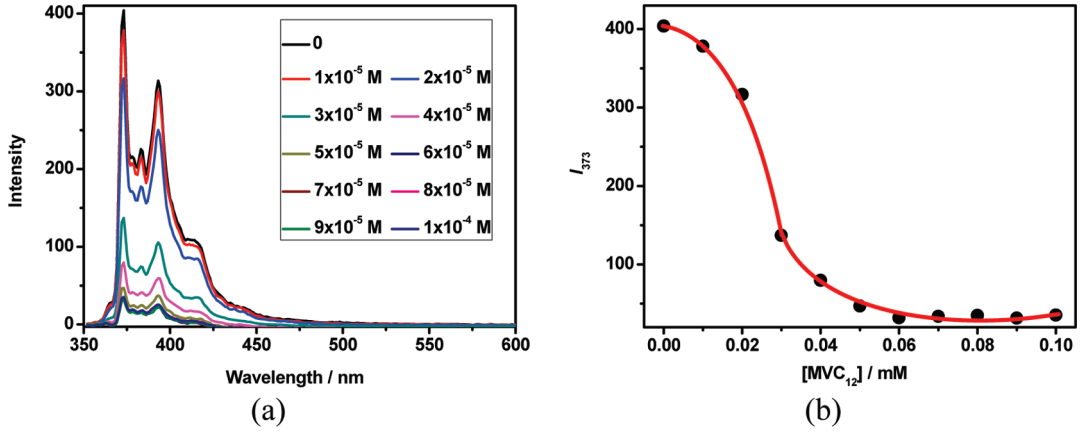

Figure 2. (a) Fluorescence emission spectra of pyrene in aqueous solutions of MVC_{12} at different concentrations in the presence of 0.02 mM C4AS at 25 °C. (b) Dependence of the relative fluorescence intensity of pyrene on MVC_{12} concentration in the presence of 0.02 mM C4AS; [pyrene] = 1.00 μM.

the electrostatic interaction between negative sulfonate groups and positive viologen groups reinforces the complex stability.

Although different concentrations of C4AS can all decrease the CAC value of MVC_{12} pronouncedly, it is still necessary to determine the best molar fraction of C4AS leading to aggregation. Figure 4a and Supporting Information, Figure S4a show the absorbance evolution at 450 nm as a function of C4AS concentration with a fixed MVC_{12} concentration at 0.08 mM, which undergoes a sharp increase and then an inverse decrease upon gradual addition of C4AS. In the left-hand portion of inflection, C4AS and MVC_{12} form a higher-order complex with a tendency toward amphiphilic aggregation, whereas in the right-hand portion of inflection, excess C4AS leads to the formation of a simple 1:1 inclusion complex rather than

higher-order aggregation. The inflection appears at the C4AS/MVC_{12} molar ratio of 0.5. The same result was also obtained by monitoring the relative fluorescence intensity of pyrene probe molecules (Figure 4b and Supporting Information, Figure S4b). That is, the charge-matching molar ratio is most suitable for amphiphilic aggregation of C4AS + MVC_{12} system.

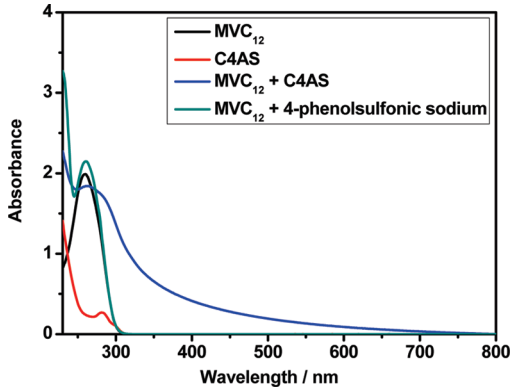

Figure 3. UV−vis absorption spectra of MVC_{12}, C4AS, MVC_{12} + C4AS, and MVC_{12} + 4-phenolsulfonic sodium at 25 °C in water; [MVC_{12}] = 0.08 mM, [C4AS] = 0.04 mM, [4-phenolsulfonic sodium] = 0.20 mM.

As can be seen from Figure 5a, a solution of C4AS + MVC_{12} presents a curved surface arising from the decrease of surface tension, and concurrently, exhibits a clear Tyndall effect, indicating the existence of abundant nanoparticles. Similar phenomena are not observed for the solution of free MVC_{12}, revealing that free MVC_{12} blocks cannot form nanoscale aggregates under the same conditions. The distinguishable amphiphilic behaviors were further reinforced by the surface tension measurements (Figure 5b). In the presence of C4AS, the surface tension of the solution decreases dramatically upon adding MVC_{12} until a maximum is reached, and after that C4AS + MVC_{12} amphiphiles start to aggregate in aqueous solution. However, in the absence of C4AS, the surface tension does not change with the increasing MVC_{12} concentration from 0.01 to 0.10 mM.

Furthermore, dynamic laser scattering (DLS) and transmission electron microscopy (TEM) were employed to identify the size and morphology of amphiphilic aggregation of C4AS + MVC_{12}. DLS result shows that the C4AS + MVC_{12} complex forms spectacular aggregates with a narrow size distribution, giving an

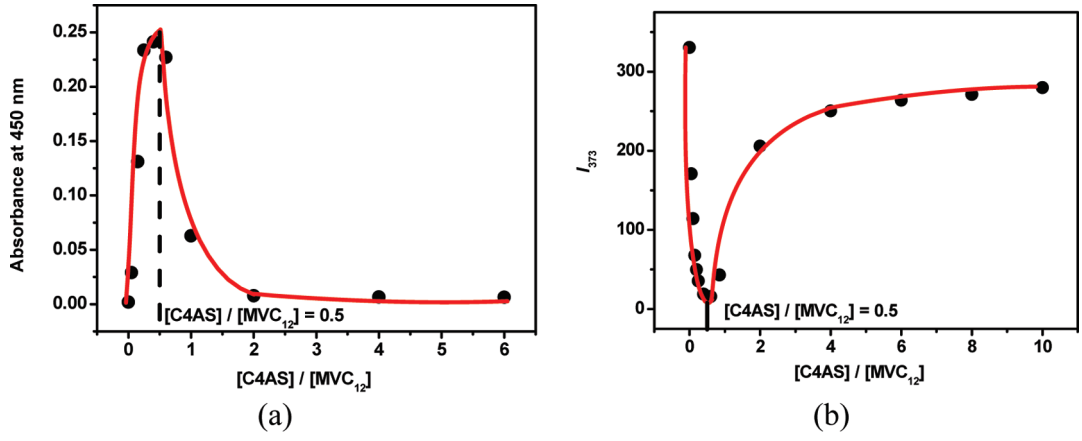

Figure 4. Dependence of the absorbance at 450 nm (a) and dependence of the relative fluorescence intensity of pyrene (b) on C4AS concentration with a fixed MVC_{12} concentration of 0.08 mM at 25 °C, [pyrene] = 1.00 μM.

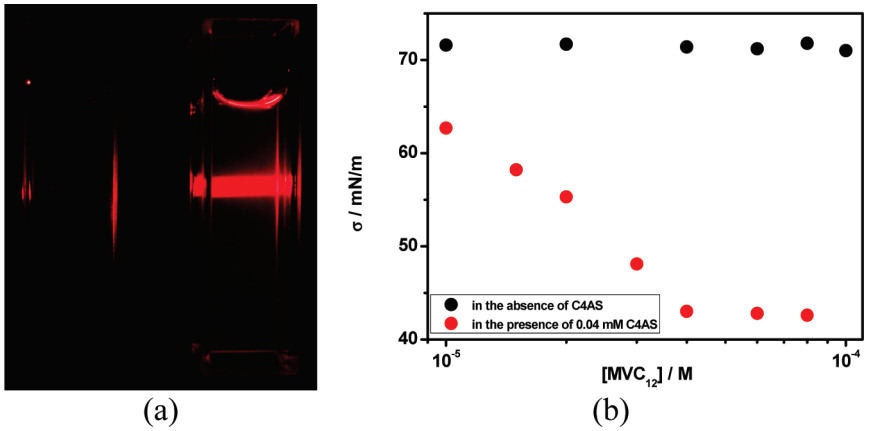

Figure 5. (a) Tyndall effect of free MVC_{12} (left) and C4AS + MVC_{12} complex (right), [MVC_{12}] = 0.08 mM, [C4AS] = 0.04 mM. (b) Surface tension data as a function of MVC_{12} concentration in the absence and in the presence of 0.04 mM C4AS at 25 °C in water.

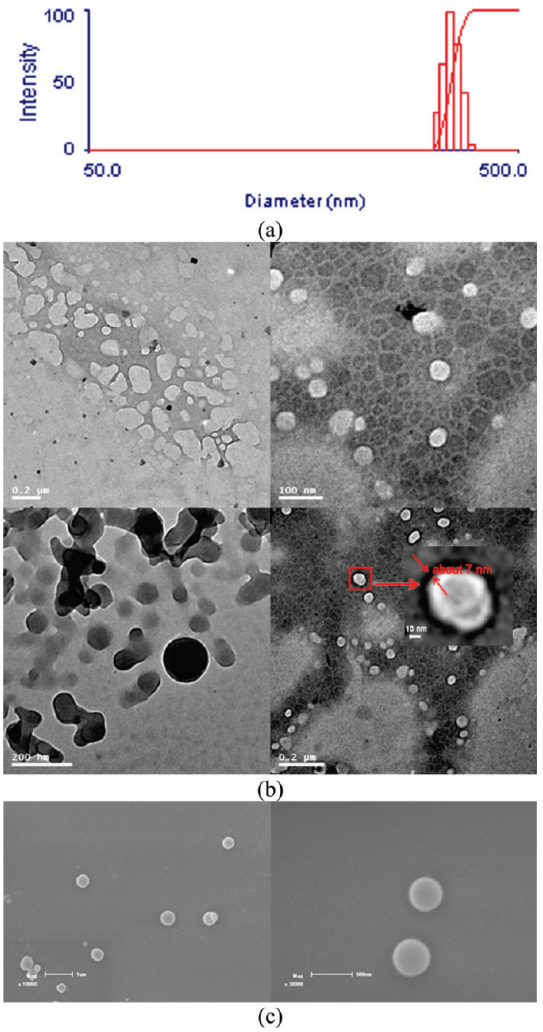

Figure 6. (a) DLS data of C4AS + MVC_{12} aggregation. TEM (b) and SEM (c) images of C4AS + MVC_{12} aggregation.

average diameter of 362 nm (Figure 6a). TEM images show the hollow spherical morphology with a diameter ranging from 50 to 400 nm, indicating convincingly the vesicular structure (Figure 6b). Such spheres are also found in scanning electron microscopy (SEM) images (Figure 6c). Moreover, from the distinguishably dark periphery and light central parts in the TEM images, we obtain the thickness of the bilayer membrane as about 7 nm, which is almost equal to the sum of two MVC_{12} lengths and two C4AS heights.[76,77] Combining all of the aforementioned results, we deduced the model of forming supramolecular binary vesicles as that illustrated in Scheme 2. The hydrophobic alkyl chains in MVC_{12} are packed together, and the inner- and outer-layer surfaces consist of hydrophilic phenolic hydroxyl groups of C4AS, which are exposed to water. C4AS and MVC_{12} are connected together by host–guest interactions.

Multistimuli-Response of the Supramolecular Binary Vesicles. The obtained supramolecular binary vesicles have the capability of responding to three external stimuli,

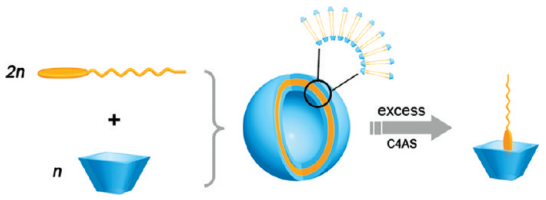

Scheme 2. Schematic representation of the construction of a supramolecular binary vesicle based on the host–guest complexation of C4AS with MVC_{12}.

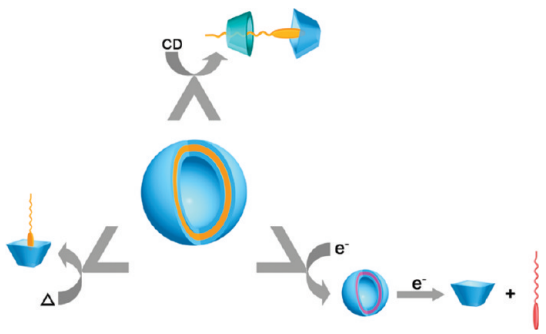

Scheme 3. Schematic representation of the multistimuli-response of supramolecular binary vesicles.

including temperature, host–guest inclusion, and redox (Scheme 3). As shown in Figure 7a and Supporting Information, Figure S5, the absorbance at 450 nm increases gradually with temperature descending from 70 to 5 °C, and decreases inversely with temperature ascending from 5 to 70 °C, which reflects the processes of assembly and disassembly, respectively. The left assembly curve is almost symmetric to the right disassembly one. The similar phenomenon is also observed for the relative fluorescence intensity of pyrene probe molecules. The intensity of pyrene fluorescence emission decreases gradually with temperature descending from 70 to 5 °C, and increases inversely with temperature ascending from 5 to 70 °C (Figure 7b and Supporting Information, Figure S6). Fluorescence control experiments were carried out with pyrene only at 5 and 70 °C and no such variation occurred (Supporting Information, Figure S7). The fluorescence changes imply the capture/release process of pyrene by vesicles. The reversible assembly/disassembly process can be modulated repeatedly several times (Figure 7c and Supporting Information, Figure S8). More powerful evidence for the disassembly of the vesicles comes from the DLS measurements (Figure 7d), showing that the scattering intensity decreases sharply when the temperature increases from 15 to 70 °C. As shown in Figure 7e, the average diameters of C4AS + MVC_{12} aggregation at 15, 25, and 45 °C are similar, and they are 359, 362, and 319 nm, respectively; however, no particle size was measured at 70 °C. These results indicate that the number of C4AS + MVC_{12} aggregations decreases sharply with increasing temperature accompanied by the gradual disassembly of the vesicles, as a result, the scattering intensity decreases sharply when

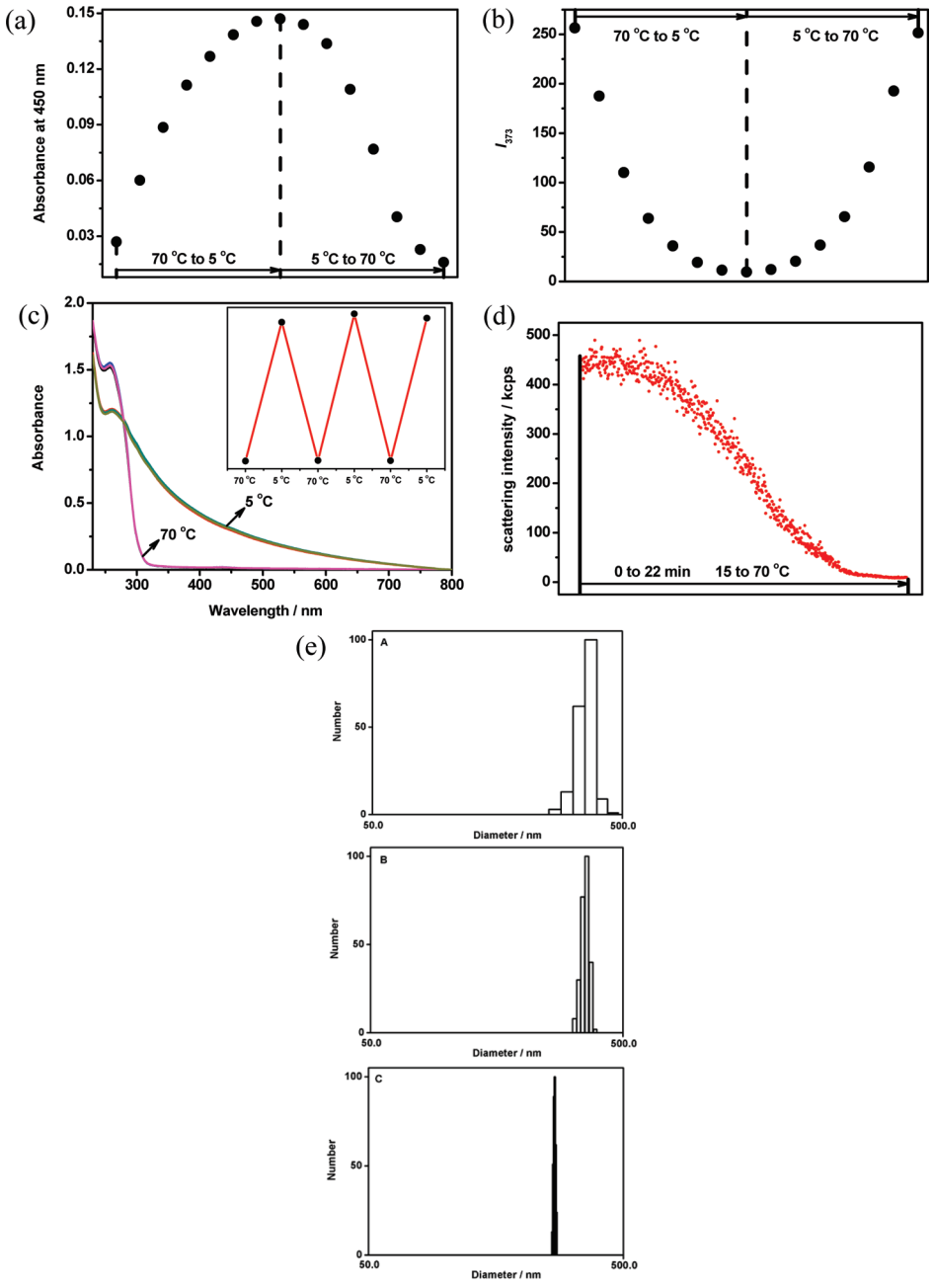

Figure 7. (a) Dependence of the absorbance of C4AS + MVC_{12} aggregation at 450 nm on temperature. (b) Dependence of the relative fluorescence intensity of pyrene in aqueous solution of C4AS + MVC_{12} aggregation on temperature. (c) UV−vis absorption spectra of C4AS + MVC_{12} aggregation observed upon several cycles of thermal equilibration at 5 and 70 °C. Inset: absorbance changes at 450 nm. (d) Evolution of scattering intensity for the C4AS + MVC_{12} aggregation as a function of time and temperature. (e) DLS results of C4AS + MVC_{12} aggregation at 15 (A), 25 (B), and 45 °C (C). [MVC_{12}] = 0.08 mM, [C4AS] = 0.04 mM, [pyrene] = 1.00 μM.

the temperature increases from 15 to 70 °C; however, the size of C4AS + MVC_{12} aggregation changes a little. The temperature response of the vesicle is acceptable for both the complexation of sulfonatocalixarenes with organic guests and the $\pi\cdots\pi$ stacking of aromatic compounds because they are enthalpy-driven processes, which would be weakened upon warming.[58,78−83] The final disassembled products may be water-soluble C4AS, MVC_{12}, and C4AS + MVC_{12} 1:1 complex according to the thermodynamic parameters for 1:1 intermolecular complexation of viologen with C4AS.[81] It is mentioned here that the assembly/disassembly process can be accomplished in the time scale of minutes with changing temperature, which endows the vesicle with kinetic availability for carry/release of special substrates.

It is well-established that the alkyl chain moiety is able to form complexes with cyclodextrins (CDs). Here we have exploited the propensity of CDs to form complexes with MVC_{12} to modulate the hydrophobicity of the alkyl chain moiety of MVC_{12}, thereby leading

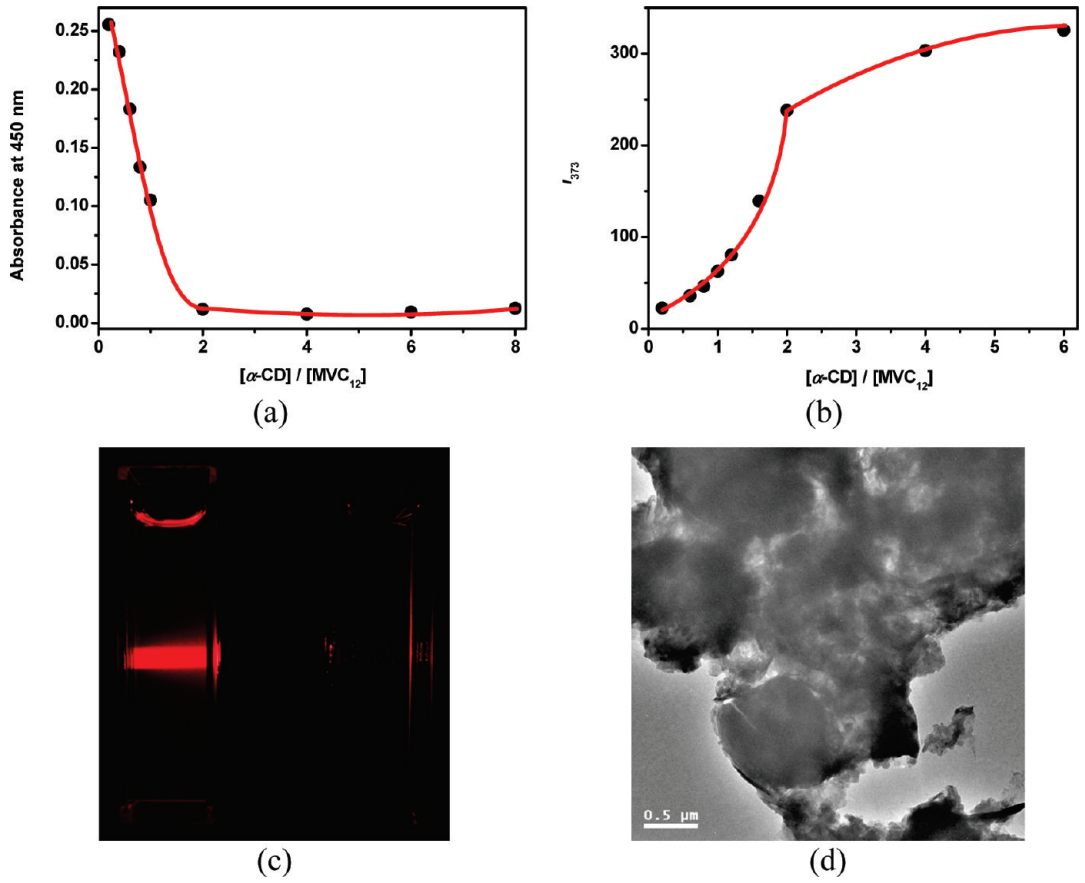

Figure 8. (a) Dependence of the absorbance of C4AS + MVC_{12} aggregation at 450 nm on α-CD concentration. (b) Dependence of the relative fluorescence intensity of pyrene in aqueous solution of C4AS + MVC_{12} aggregation on α-CD concentration. (c) Tyndall effect of C4AS + MVC_{12} aggregation in the absence (left) and in the presence (right) of excess α-CD. (d) TEM image of C4AS + MVC_{12} aggregation in the presence of excess α-CD. [MVC_{12}] = 0.08 mM, [C4AS] = 0.04 mM, [α-CD] = 0.32 mM, [pyrene] = 1.00 μM.

to the disassembly of the vesicle architecture. As shown in Figure 8a and Supporting Information, Figure S9a, the absorbance of C4AS + MVC_{12} aggregation at 450 nm decreases dramatically upon gradual addition of α-CD, and *ca.* 2 equiv of α-CD is required to fully disrupt the vesicles. It is also observed for the relative fluorescence intensity of pyrene probe molecules. As can be seen in Figure 8b and Supporting Information, Figure S9b, adding α-CD to the solution increases the intensity of fluorescence emission, which levels off after the addition of *ca.* 2 equiv of α-CD. An alternative rationalization of the data in Figure 8b would assume the formation of pyrene + α-CD complex; however, this possibility must be ruled out because the pyrene molecule is too large to fit inside the α-CD cavity (Supporting Information, Figure S10).[84] The Tyndall effect for C4AS + MVC_{12} solution disappears after adding excess α-CD accompanied by a dramatic decrease of scattering intensity measured by DLS (Figure 8c). Concurrently, no vesicle could be found in TEM images any more (Figure 8d). All these results indicate the disassembly of the C4AS + MVC_{12} binary vesicles upon adding α-CD. The complexation-driven disruption of the vesicle is presumably due to an increase in the hydrophilic nature of alkyl chain upon immersion into the cavity of α-CD.

Similar experimental phenomena can also be observed by adding β- or γ-CD (Figure 9). The only difference is that compared with α-CD, more β- or γ-CD is required to fully disrupt the vesicles (*ca.* 3 equiv). A rational explanation is that α-CD has a stronger binding ability toward the alkyl chain moiety than β- and γ-CD.[72] The comparison among α-, β-, and γ-CD further validates the issue that the CD-induced disruption of C4AS + MVC_{12} vesicle is a complexation-driven process.

It is well-known that viologens can be transformed into the corresponding radical cations and neutral molecules either chemically or electrochemically. It is expected that the binary vesicle can be modulated by one- or two-step reduction of MVC_{12} because C4AS exhibits distinguishable binding affinities toward viologen dication, radical cation, and neutral form, respectively.[81] As shown in Figure 10a, when excess hydrazine was added to the solution of MVC_{12}, a new band at about 600 nm appears corresponding to the radical cation state of MVC_{12}, and concurrently, the solution color changes from colorless to blue (Figure 10b). However, in the case of C4AS + MVC_{12}, it shows the characteristic absorption of the dimeric (or oligomeric) species of viologen radical cation when hydrazine was added, and the solution color changes to purple.[77,85] The purple solution is much more

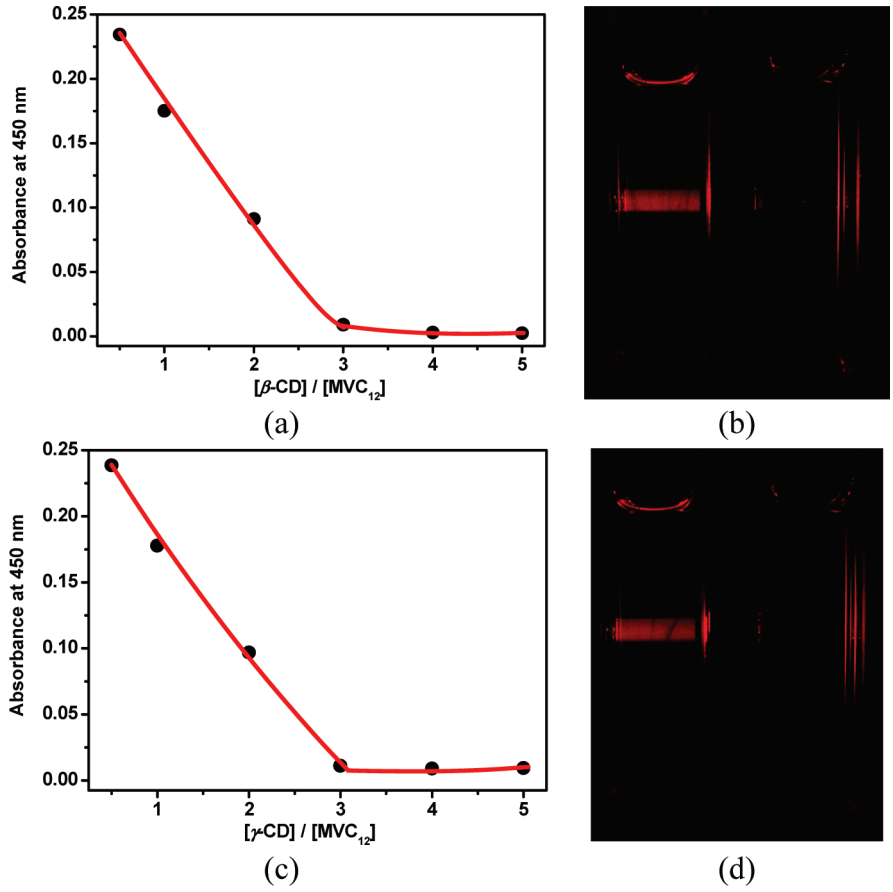

Figure 9. (a) Dependence of the absorbance of C4AS + MVC_{12} aggregation at 450 nm on β-CD concentration. (b) Tyndall effect of C4AS + MVC_{12} aggregation in the absence (left) and in the presence (right) of excess β-CD. (c) Dependence of the absorbance of C4AS + MVC_{12} aggregation at 450 nm on γ-CD concentration. (d) Tyndall effect of C4AS + MVC_{12} aggregation in the absence (left) and in the presence (right) of excess γ-CD. [MVC_{12}] = 0.08 mM, [C4AS] = 0.04 mM, [β-CD] = 0.32 mM, [γ-CD] = 0.32 mM.

stable than the blue one when exposed to the air. Control experiments were carried out with methyl viologen in the absence and in the presence of C4AS, and no such difference was found after reduction by hydrazine. This implies that the C4AS + MVC_{12} system still exists in aggregation form after reduction of MVC_{12} to its radical cation state, also proved by the Tyndall effect (Figure 11a). Differently, the average diameter of the resulting particles decreases to 153 nm (Figure 11b). TEM images confirm these particles are also vesicles after reduction (Figure 11c). Interestingly, DLS measurements show that the initial vesicle can be recovered (average diameter of 308 nm) after reoxidation of MVC_{12} radical cation state to its dication state (Figure 11b). That is, we can achieve the fascinating conversion between two sizes of vesicles reversibly, driven by chemical or electrical redox. As proved before, C4AS can also bind viologen radical cation effectively,[81] and thereby, C4AS forms supramolecular binary vesicle with MVC_{12} radical cation too. For the decrease of vesicle size upon reduction, one reasonable explanation is that the pronouncedly weakened electrostatic repulsion from dication to radical cation state is favorable for aggregation with higher curvature.

Cyclic voltammetric experiment was further performed for C4AS + MVC_{12} aggregation to demonstrate that MVC_{12} can also be transformed into its radical cation and neutral molecule in the presence of C4AS electrochemically (Supporting Information, Figure S11), which may also modify the structure of C4AS + MVC_{12} binary vesicle. As shown in Figure 12a, the Tyndall effect for C4AS + MVC_{12} aggregation disappeared after application of a reduction potential (−1.6 V *vs* Ag/AgCl) for 30 min, accompanied by a dramatic decrease of scattering intensity measured by DLS. Concurrently, no vesicle could be found in TEM images any more (Figure 12b). All these results indicate undoubtedly the disassembly of the supramolecular binary vesicles by transformation of MVC_{12} into the corresponding neutral molecules electrochemically.

Loading Model Molecule by the Vesicles and its Controllable Release. According to the multistimuli-responsive character of binary C4AS + MVC_{12} vesicles, we selected doxorubicin hydrochloride (DOX), one kind of water-soluble fluorescence dye and anticancer drug molecules, as model molecule to investigate its capability of entrapment and release. After purification by ultracentrifugation and dialysis, DOX was successfully loaded in the vesicle. In comparison with the unloaded vesicle, the absorption of loaded

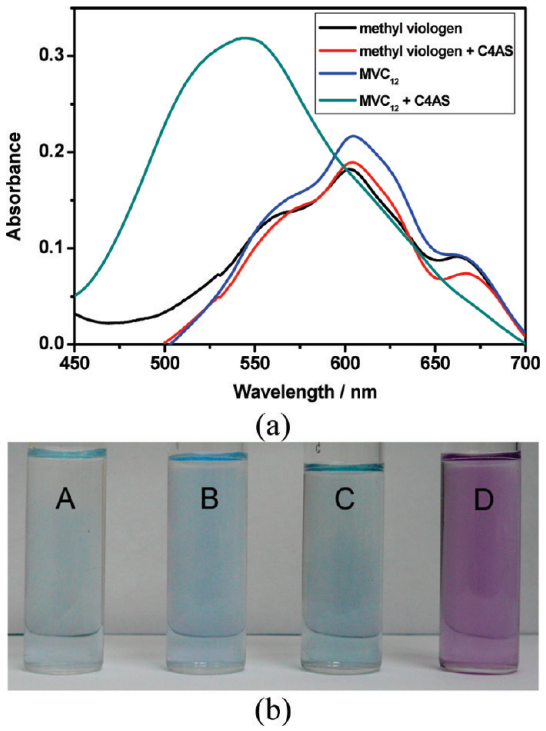

Figure 10. (a) UV−vis absorption spectra of methyl viologen, methyl viologen + C4AS, MVC_{12}, and MVC_{12} + C4AS after reduction by excess hydrazine. (b) The solution color of methyl viologen (A), methyl viologen + C4AS (B), MVC_{12} (C), and MVC_{12} + C4AS (D) after reduction by excess hydrazine. [methyl viologen] = 0.08 mM, [MVC_{12}] = 0.08 mM, [C4AS] = 0.04 mM.

vesicle becomes much stronger from 450 to 550 nm (Figure 13), which represents the characteristic absorption of DOX. Moreover, the vesicular solution turns from colorless to light red (Figure 13). According to UV−vis absorption spectra, the DOX encapsulation and loading efficiency were calculated to be 86.0% and 6.1%, respectively.

The loaded DOX molecules were successfully released upon warming, together with the disassembly of the vesicles, as proved by detecting the amplification of the fluorescence signal of DOX accompanied with temperature increase (Supporting Information, Figure S12a). The DOX-release process as a function of temperature was recorded and is shown in Figure 14a. The results show that increasing the temperature from 25 to 60 °C triggers a gradual enhancement for DOX release, reaching 100% at 60 °C. The DOX-release process, accompanied with the disassembly of the vesicle, was further reinforced by the control experiment with the addition of Triton X-100, which is known to solublize vesicles (Supporting Information, Figure S12b). It is mentioned here that the fluorescence signal of DOX itself is almost not changed with changing temperature from 25 to 60 °C (Supporting Information, Figure S13). Furthermore, UV−vis absorption spectroscopy was also used to monitor the release of DOX from DOX-loaded vesicles at 60 °C as well as with the addition of Triton X-100 by the dialysis method, the results of which are in accordance with those obtained above. No characteristic absorption of DOX from 450 to 550 nm can

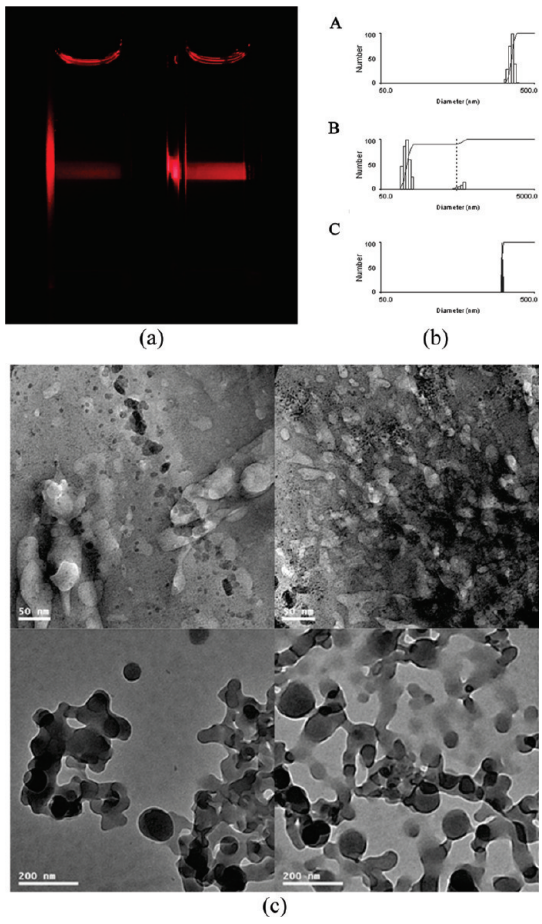

Figure 11. (a) Tyndall effect of C4AS + MVC_{12} aggregation before (left) and after (right) reduction by excess hydrazine, [MVC_{12}] = 0.08 mM, [C4AS] = 0.04 mM. (b) DLS results of C4AS + MVC_{12} aggregation (A), and its reduction (B) and reoxidation (C) products. (c) TEM images of C4AS + MVC_{12} aggregation after reduction by excess hydrazine.

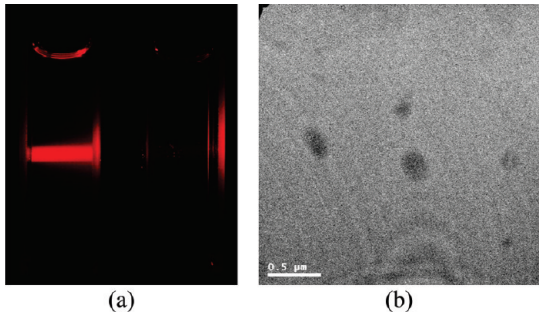

Figure 12. (a) Tyndall effect of C4AS + MVC_{12} aggregation before (left) and after (right) application of a reduction potential (−1.6 V *vs* Ag/AgCl) for 30 min, [MVC_{12}] = 0.08 mM, [C4AS] = 0.04 mM. (b) TEM image of C4AS + MVC_{12} aggregation after application of a reduction potential (−1.6 V *vs* Ag/AgCl) for 30 min.

be detected for DOX-loaded vesicles at 60 °C or with the addition of Triton X-100 after dialysis, which indicates a complete release of encapsulated DOX in the two cases accompanied by the fully disassembly of the vesicles.

In another independent experiment, as shown in Figure 14b and Supporting Information, Figure S14a, a

very low release of entrapped DOX was observed over periods of 100 h, indicating that the vesicles are highly stable toward leakage at room temperature. However, adding α-CD to the solution of DOX-loaded vesicles resulted in a rapid and complete release of encapsulated DOX (Figure 14b and Supporting Information, Figure S14b). Control experiment shows that adding α-CD to DOX solution cannot change its fluorescence signal (Supporting Information, Figure S15), indicating α-CD cannot form complex with DOX. UV−vis absorption spectroscopy was also used to monitor the release of DOX from DOX-loaded vesicles with the addition of α-CD by dialysis method and no characteristic absorption of DOX from 450 to 550 nm can be detected for DOX-loaded vesicles with the addition of α-CD after dialysis, which also indicates a complete release of encapsulated DOX upon the addition of α-CD accompanied by the fully disassembly of the vesicles.

Cellular Toxicity and Anticancer Efficiency of DOX-Loaded Vesicle. We further performed the basic cell experiments to evaluate the cellular toxicity of the supramolecular binary vesicle and the anticancer efficiency of DOX-loaded vesicle. First, unloaded vesicle, DOX, and DOX-loaded vesicle were incubated with NIH3T3 cells (normal cells), and the numbers of living cells in different groups were recorded from day 1 to day 4. As shown in Figure 15a, we found that the number of living cell in unloaded vesicle group is always much

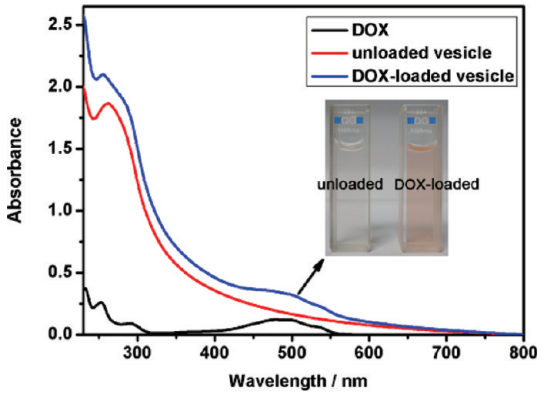

Figure 13. UV−vis absorption spectra of DOX, unloaded vesicles, and DOX-loaded vesicles at 25 °C in water. Inset: color change of DOX-loaded vesicle (right) compared with unloaded one (left).

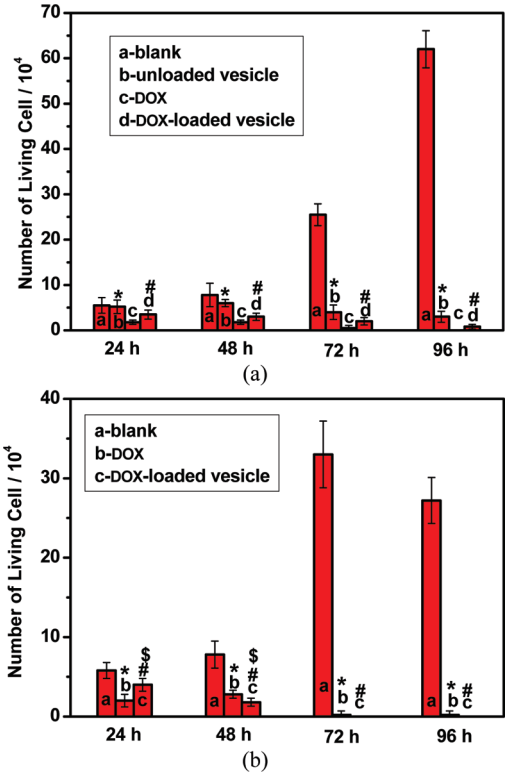

Figure 15. (a) Number of living NIH3T3 cells in blank group, and after treatment with unloaded vesicle, DOX, and DOX-loaded vesicles at different times. The asterisks indicate $P < 0.01$ *versus* DOX group and pound sign indicates $P < 0.05$ *versus* DOX group at the same time and same concentration of DOX. (b) Number of living HepG-2 cells in blank group and after treatment with DOX and DOX-loaded vesicles at different times. The asterisks and pound sign indicate $P < 0.05$ *versus* the blank group, and the dollar sign indicates $P < 0.05$ *versus* DOX group at the same time and same concentration of DOX. When the P value was less than 0.05, differences were considered statistically significant.

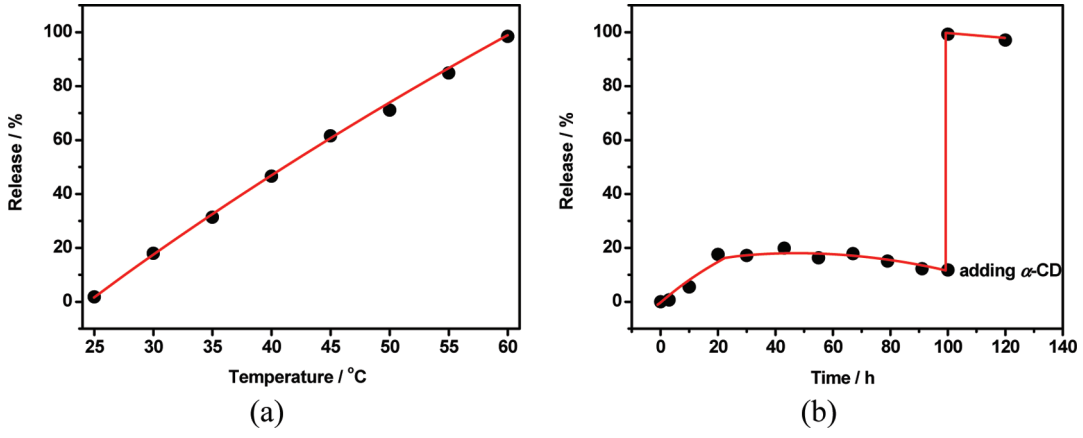

Figure 14. (a) Release percent of DOX from the loaded vesicle as a function of temperature. (b) Release percent of DOX from the loaded vesicle as a function of time.

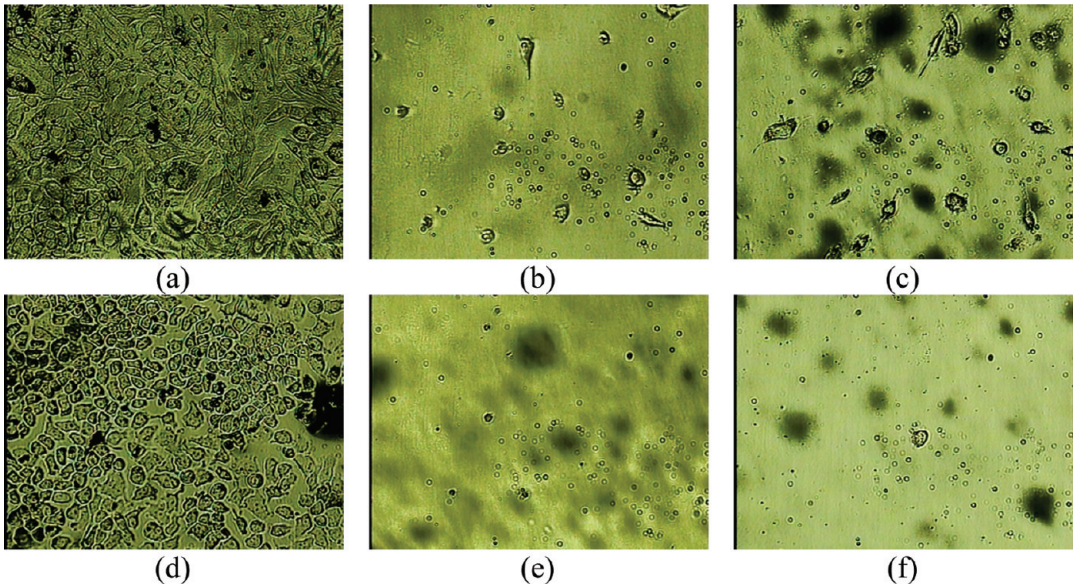

Figure 16. The images of living NIH3T3 cells in blank group (a), DOX group (b), and DOX-loaded vesicle group (c) after 96 h. The images of living HepG-2 cells in blank group (d), DOX group (e), and DOX-loaded vesicle group (f) after 96 h.

more than that in DOX group from day 1 to day 4 ($P < 0.01$), indicating undoubtedly that the cytotoxicity of unloaded vesicle was much lower compared with DOX. Moreover, it is quite interesting and meaningful that the number of living cells in the DOX-loaded vesicle group is also always much more than that in the DOX group from day 1 to day 4 ($P < 0.05$), and the morphology of living cells in the DOX-loaded vesicle group is better than that in the DOX group even after 96 h (Figure 16b,c), both of which imply that the systemic toxicity of DOX was reduced upon loading by vesicle. DOX and DOX-loaded vesicles were then incubated with HepG-2 cells (cancer cells), and the numbers of living cells in different groups were also recorded from day 1 to day 4. As shown in Figure 15b, we found that the numbers of living cells in both the DOX group and the DOX-loaded vesicle group are always much less than that in the blank group from day 1 to day 4 ($P < 0.05$). Furthermore, both the numbers of living cells from day 1 to day 4 (Figure 15b) and cell images after 96 h (Figure 16e,f) for the DOX group and DOX-loaded vesicle group showed that no obvious difference about therapeutic effects of DOX group and DOX-loaded vesicle group against cancer cells was found. It can be seen that loading of DOX by vesicle does not affect the therapeutic effect of DOX for cancer cells. However, its damage for normal cells is reduced. One reasonable explanation is that anticancer drug DOX has a stronger interaction with cancer cells than with normal cells, and then the release of DOX from vesicle to cancer cell is more efficient than that to normal cell.

CONCLUSIONS

We have successfully constructed self-assembled nanosupramolecular binary vesicles based on host–guest complexation, employing C4AS as the host and MVC_{12} as the guest, respectively. The CAC value of MVC_{12} decreases pronouncedly by a factor of *ca.* 1000 due to the complexation of C4AS. More noticeably, the obtained vesicle is multistimuli-responsive, benefiting from the intrinsic advantages of supramolecules. Reduction of MVC_{12} to radical cation state can adjust the vesicle to smaller species and *vice versa*. Reduction to neutral form, increasing temperature, and inclusion of CDs can all lead to the vesicle disruption completely. All these external stimuli can act as an effective switch that triggers the efficient release of the entrapped substrates. In addition, cell experiments show that the loading of DOX by a vesicle does not affect the therapeutic effect of DOX for cancer cells, whereas its damage for normal cells is reduced. The present results not only pave an alternative way to build novel supramolecular vesicles, but also endow vesicle multistimuli responsiveness for the first time. Such smart self-assembled modeling materials promise substantial application in the fields of controlled release and drug delivery.

METHODS

Materials Preparation. Pyrene and 4-phenolsulfonic sodium were commercially available from Acros. Hydrazine and doxorubicin hydrochloride were commercially available from Aladdin. The α-, β-, and γ-cyclodextrins were purchased from TCI. All of these were used without further purification. Methyl viologen, asymmetric viologen, and *p*-sulfonatocalix[4]arene were synthesized and purified according to previously reported procedures,[81,86,87]

and they were identified by ^{1}H NMR spectroscopy in D_2O, performed on a Varian 300 spectrometer, mass spectrometry, performed on an IonSpec QFT-ESI MS, and elemental analysis, performed on a Perkin−Elmer-2400C instrument.

DOX-Loaded Vesicle. DOX-loaded vesicles were prepared as follows: A certain amount of DOX was added to a solution containing C4AS and MVC_{12}, and then some water was added until the volume of the solution reached 25 mL. The ultimate concentrations of DOX, C4AS, and MVC_{12} were 0.01, 0.04, and 0.08 mM, respectively. Subsequently, the prepared DOX-loaded vesicles were purified by ultracentrifugation (10000 rpm for 2 min) and dialysis (molecular weight cutoff = 3500) in distilled water for several times until the water outside the dialysis tube exhibited negligible DOX fluorescence.

The DOX encapsulation and loading efficiency were calculated by the following equations:

$$\text{encapsulation efficiency}\ (\%) = (m_{\text{DOX-loaded}}/m_{\text{DOX}})100 \quad (1)$$

$$\text{loading efficiency}\ (\%) = (m_{\text{DOX-loaded}}/m_{\text{NPs}})100 \quad (2)$$

$m_{\text{DOX-loaded}}$, m_{DOX}, and m_{NPs} are mass of DOX encapsulated in vesicles, mass of DOX added, and mass of DOX-loaded vesicles, respectively. The mass of DOX was measured by a UV spectrophotometer at 490 nm and calculated as relative to a standard calibration curve in the concentrations from 3.82 to 22.92 μg/mL in water.

Controllable DOX release. An excitation wavelength of 500 nm and an emission wavelength of 589 nm were used. The initial fluorescence intensity (F_0) of DOX-loaded vesicles was measured by using a fluorescence spectrometer, and then the fluorescence intensity (F_T) of DOX-loaded vesicles was measured as a function of temperature. The temperature treatment time for determination is 5 min for every temperature point. In another independent experiment, the fluorescence intensity (F_t) of DOX-loaded vesicles was measured as a function of time. Next, the fluorescence intensity (F_{CD}) of DOX-loaded vesicles after adding α-CD was measured. Finally, to confirm the overall intensity (F_{Triton}), more DOX-loaded vesicles were completely disrupted by adding Triton X-100. The release percentage of DOX-loaded vesicles was calculated by using eq 3:

$$\text{release percentage}\ (\%) = ((F_{\text{T(t)(CD)}} - F_0)/(F_{\text{Triton}} - F_0))100 \quad (3)$$

The reason for the quenching of fluorescence emission of DOX in the vesicles may be the self-quenching originating from its relatively high concentration in the vesicles or the photoinduced electron transfer from the oxygen anion at the lower-rim of C4AS to DOX. The pH value for this C4AS + MVC_{12} system is 5.31. According to the pK_a values of lower-rim phenolic hydroxyl groups of C4AS (pK_a values =3.08, 12.02),[88] at least one phenol group is deprotonated at this pH value.

The release of DOX from DOX-loaded vesicles at 60 °C, with the addition of Triton X-100, and with the addition of α-CD by dialysis method was performed as follows: The DOX-loaded vesicles at 60 °C, with the addition of Triton X-100, or with the addition of excess α-CD were dialyzed (molecular weight cutoff = 3500) against the deionized water for several times until the water outside the dialysis tube exhibited negligible DOX fluorescence. And then, the inner solution was taken, and its DOX content was measured *via* absorbance at 490 nm.

UV−vis Absorption and Fluorescence Emission Spectra. UV−vis spectra were recorded in a quartz cell (light path 10 mm) on a Shimadzu UV-3600 spectrophotometer equipped with a PTC-348WI temperature controller. Steady-state fluorescence spectra were recorded in a conventional quartz cell (light path 10 mm) on a Varian Cary Eclipse equipped with a Varian Cary single-cell peltier accessory to control temperature. λ_{ex} = 335.0 nm; bandwidth (ex), 10 nm; bandwidth (em), 2.5 nm, unless otherwise stated.

Surface Tension Measurements. The static surface tension in aqueous solution was measured by using a QBZY full-automatic surface tensiometer by the method of platinum plate at 25 °C.

TEM and SEM Experiments. TEM images were recorded on a Philips Tecnai G2 20S-TWIN microscope operating at an accelerating voltage of 200 keV. The sample for TEM measurements was prepared by dropping the solution onto a copper grid. The grid was then air-dried. SEM images were recorded on a Hitachi S-3500N SEM. The sample for SEM measurements was prepared by dropping the solution onto a coverslip, followed by evaporating the liquid in air. The concentrations of C4AS and MVC_{12} were 0.04 and 0.08 mM, respectively.

DLS Measurements. The sample solution for DLS measurements was prepared by filtering solution through a 450 nm Millipore filter into a clean scintillation vial. The samples were examined on a laser light scattering spectrometer (Bl-200SM) equipped with a digital correlator (Turbo Corr.) at 532 nm at a scattering angle of 90°. The concentrations of C4AS and MVC_{12} were 0.04 and 0.08 mM, respectively.

Electrochemical Experiments. The cyclic voltammetric measurements were carried out on a BAS Epsilon electrochemical analyzer with C3 cell stand. All the samples were prepared in aqueous solutions at 25 °C, and deoxygenated by purging with dry nitrogen before each experiment. The glassy carbon working electrode was polished with 0.05 μm BAS alumina suspension on a brown Texmet polishing pad, sonicated in distilled water for a few minutes to remove any residual alumina particles, and then rinsed with ethanol before use. A platinum wire was used as the counter electrode. The measured potentials were recorded with respect to an Ag/AgCl (immersed in a solution containing 3 M sodium chloride) reference electrode. The concentrations of C4AS and MVC_{12} were 0.04 and 0.08 mM, respectively. The scan rate is 10 mV/s.

The electrochemical reduction of C4AS + MVC_{12} aggregation was performed as follows: a thin platinum plate (as working electrode) was placed in a 1.0 cm cell, to which 3.0 mL of C4AS + MVC_{12} aggregation solution was added. A platinum wire as counter electrode and an Ag/AgCl electrode as reference electrode were carefully inserted into the solution. And then a reduction potential (−1.6 V *vs* Ag/AgCl) was applied for the sample for 30 min. The concentrations of C4AS and MVC_{12} were 0.04 and 0.08 mM, respectively.

Cell Experiments. NIH3T3 and HepG-2 cells were seeded in clear 24-well plates at a density of 10^4 cells/well in 1000 μL of complete DMEM and 10% FCS, and grown for 24 h at 37 °C. NIH3T3 cells were subsequently incubated with unloaded vesicle, DOX, and DOX-loaded vesicle. HepG-2 cells were subsequently incubated with DOX and DOX-loaded vesicle. The ultimate concentrations of DOX, C4AS, and MVC_{12} were 0.01, 0.04, and 0.08 mM, respectively. After another 24, 48, 72, and 96 h incubation, the number of living cells in every group was measured. The number of living cells is expressed as the mean ± standard deviation and *t*-test was used for statistical analysis of the data. Differences were considered statistically significant when the *P* value was less than 0.05.

Acknowledgment. This work was supported by 973 Program (2011CB932502) and NNSFC (Nos. 20703025 and 20932004), which are gratefully acknowledged.

Supporting Information Available: Experimental details indicated in the manuscript. This material is available free of charge *via* the Internet at http://pubs.acs.org.

REFERENCES AND NOTES

1. Zhou, S.; Burger, C.; Chu, B.; Sawamura, M.; Nagahama, N.; Toganoh, M.; Hackler, U. E.; Isobe, H.; Nakamura, E. Spherical Bilayer Vesicles of Fullerene-Based Surfactants in Water: A Laser Light Scattering Study. *Science* **2001,** *291*, 1944–1947.
2. Discher, D. E.; Eisenberg, A. Polymer Vesicles. *Science* **2002,** *297*, 967–973.
3. Zhang, X.; Rehm, S.; Safont-Sempere, M. M.; Würthner, F. Vesicular Perylene Dye Nanocapsules as Supramolecular Fluorescent pH Sensor Systems. *Nat. Chem.* **2009,** *1*, 623–629.
4. Mueller, A.; O'Brien, D. F. Supramolecular Materials *via* Polymerization of Mesophases of Hydrated Amphiphiles. *Chem. Rev.* **2002,** *102*, 727–757.
5. Vriezema, D. M.; Aragonès, M. C.; Elemans, J. A. A. W.; Cornelissen, J. J. L. M.; Rowan, A. E.; Nolte, R. J. M. Self-Assembled Nanoreactors. *Chem. Rev.* **2005,** *105*, 1445–1489.

6. Kolusheva, S.; Shahal, T.; Jelinek, R. Cation-Selective Color Sensors Composed of Ionophore–Phospholipid–Polydiacetylene Mixed Vesicles. *J. Am. Chem. Soc.* **2000,** *122*, 776–780.
7. Kunitake, T. Synthetic Bilayer Membranes: Molecular Design, Self-Organization, and Application. *Angew. Chem., Int. Ed.* **1992,** *31*, 709–726.
8. Cassell, A. M.; Asplund, C. L.; Tour, J. M. Self-Assembling Supramolecular Nanostructures from a C_{60} Derivative: Nanorods and Vesicles. *Angew. Chem., Int. Ed.* **1999,** *38*, 2403–2405.
9. Brettreich, M.; Burghardt, S.; Böttcher, C.; Bayerl, T.; Bayerl, S.; Hirsch, A. Globular Amphiphiles: Membrane-Forming Hexaadducts of C_{60}. *Angew. Chem., Int. Ed.* **2000,** *39*, 1845–1848.
10. Renkes, T.; Schäfer, H. J.; Siemens, P. M.; Neumann, E. Fatty Acid-Oligo(ethylene glycol) Ester Forms Ion Channels in Lipid Membranes. *Angew. Chem., Int. Ed.* **2000,** *39*, 2512–2516.
11. Ravoo, B. J.; Darcy, R. Cyclodextrin Bilayer Vesicles. *Angew. Chem., Int. Ed.* **2000,** *39*, 4324–4326.
12. Dwars, T.; Paetzold, E.; Oehme, G. Reactions in Micellar Systems. *Angew. Chem., Int. Ed.* **2005,** *44*, 7174–7199.
13. Guo, X.; Szoka, F. C. Chemical Approaches to Triggerable Lipid Vesicles for Drug and Gene Delivery. *Acc. Chem. Res.* **2003,** *36*, 335–341.
14. Zhu, J.; Munn, R. J.; Nantz, M. H. Self-Cleaving Ortho Ester Lipids: A New Class of pH-Vulnerable Amphiphiles. *J. Am. Chem. Soc.* **2000,** *122*, 2645–2646.
15. Johnsson, M.; Wagenaar, A.; Engberts, J. B. F. N. Sugar-Based Gemini Surfactant with a Vesicle-to-Micelle Transition at Acidic pH and a Reversible Vesicle Flocculation near Neutral pH. *J. Am. Chem. Soc.* **2003,** *125*, 757–760.
16. Lee, M.; Lee, S.-J.; Jiang, L.-H. Stimuli-Responsive Supramolecular Nanocapsules from Amphiphilic Calixarene Assembly. *J. Am. Chem. Soc.* **2004,** *126*, 12724–12725.
17. Chécot, F.; Lecommandoux, S.; Gnanou, Y.; Klok, H.-A. Water-Soluble Stimuli-Responsive Vesicles from Peptide-Based Diblock Copolymers. *Angew. Chem., Int. Ed.* **2002,** *41*, 1339–1343.
18. Sumida, Y.; Masuyama, A.; Takasu, M.; Kida, T.; Nakatsuji, Y.; Ikeda, I.; Nojima, M. New pH-Sensitive Vesicles. Release Control of Trapped Materials from the Inner Aqueous Phase of Vesicles Made from Triple-Chain Amphiphiles Bearing Two Carboxylate Groups. *Langmuir* **2001,** *17*, 609–612.
19. Drummond, D. C.; Zignani, M.; Leroux, J.-C. Current Status of pH-Sensitive Liposomes in Drug Delivery. *Prog. Lipid Res.* **2000,** *39*, 409–460.
20. Park, C.; Lee, I. H.; Lee, S.; Song, Y.; Rhue, M.; Kim, C. Cyclodextrin-Covered Organic Nanotubes Derived from Self-Assembly of Dendrons and Their Supramolecular Transformation. *Proc. Natl. Acad. Sci. U.S.A* **2006,** *103*, 1199–1203.
21. Rodríguez-Hernández, J.; Lecommandoux, S. Reversible Inside-Out Micellization of pH-Responsive and Water-Soluble Vesicles Based on Polypeptide Diblock Copolymers. *J. Am. Chem. Soc.* **2005,** *127*, 2026–2027.
22. Du, J.; Tang, Y.; Lewis, A. L.; Armes, S. P. pH-Sensitive Vesicles Based on a Biocompatible Zwitterionic Diblock Copolymer. *J. Am. Chem. Soc.* **2005,** *127*, 17982–17983.
23. Liu, X.; Jiang, M. Optical Switching of Self-Assembly: Micellization and Micelle–Hollow-Sphere Transition of Hydrogen-Bonded Polymers. *Angew. Chem., Int. Ed.* **2006,** *45*, 3846–3850.
24. Wang, C.; Chen, Q.; Xu, H.; Wang, Z.; Zhang, X. Photoresponsive Supramolecular Amphiphiles for Controlled Self-Assembly of Nanofibers and Vesicles. *Adv. Mater.* **2010,** *22*, 2553–2555.
25. Li, Y.; Lokitz, B. S.; McCormick, C. L. Thermally Responsive Vesicles and Their Structural "Locking" through Polyelectrolyte Complex Formation. *Angew. Chem., Int. Ed.* **2006,** *45*, 5792–5795.
26. Qin, S.; Geng, Y.; Discher, D. E.; Yang, S. Temperature-Controlled Assembly and Release from Polymer Vesicles of Poly(ethylene oxide)-*block*-poly(*N*-isopropylacrylamide). *Adv. Mater.* **2006,** *18*, 2905–2909.
27. He, J.; Tong, X.; Tremblay, L.; Zhao, Y. Corona-Cross-Linked Polymer Vesicles Displaying a Large and Reversible Temperature-Responsive Volume Transition. *Macromolecules* **2009,** *42*, 7267–7270.
28. Napoli, A.; Valentini, M.; Tirelli, N.; Müller, M.; Hubbell, J. A. Oxidation-Responsive Polymeric Vesicles. *Nat. Mater.* **2004,** *3*, 183–189.
29. Yan, Q.; Yuan, J.; Cai, Z.; Xin, Y.; Kang, Y.; Yin, Y. Voltage-Responsive Vesicles Based on Orthogonal Assembly of Two Homopolymers. *J. Am. Chem. Soc.* **2010,** *132*, 9268–9270.
30. Power-Billard, K. N.; Spontak, R. J.; Manners, I. Redox-Active Organometallic Vesicles: Aqueous Self-Assembly of a Diblock Copolymer with a Hydrophilic Polyferrocenylsilane Polyelectrolyte Block. *Angew. Chem., Int. Ed.* **2004,** *43*, 1260–1264.
31. Kim, E.; Kim, D.; Jung, H.; Lee, J.; Paul, S.; Selvapalam, N.; Yang, Y.; Lim, N.; Park, C. G.; Kim, K. Facile, Template-Free Synthesis of Stimuli-Responsive Polymer Nanocapsules for Targeted Drug Delivery. *Angew. Chem., Int. Ed.* **2010,** *49*, 4405–4408.
32. Wang, C.; Guo, Y.; Wang, Y.; Xu, H.; Zhang, X. Redox Responsive Supramolecular Amphiphiles Based on Reversible Charge Transfer Interactions. *Chem. Commun.* **2009,** 5380–5382.
33. Klaikherd, A.; Nagamani, C.; Thayumanavan, S. Multistimuli Sensitive Amphiphilic Block Copolymer Assemblies. *J. Am. Chem. Soc.* **2009,** *131*, 4830–4838.
34. Beck, J. B.; Rowan, S. J. Multistimuli, Multiresponsive Metallo-Supramolecular Polymers. *J. Am. Chem. Soc.* **2003,** *125*, 13922–13923.
35. Wang, C.; Chen, Q.; Sun, F.; Zhang, D.; Zhang, G.; Huang, Y.; Zhao, R.; Zhu, D. Multistimuli Responsive Organogels Based on a New Gelator Featuring Tetrathiafulvalene and Azobenzene Groups: Reversible Tuning of the Gel–Sol Transition by Redox Reactions and Light Irradiation. *J. Am. Chem. Soc.* **2010,** *132*, 3092–3096.
36. Oishi, M.; Nakamura, T.; Jinji, Y.; Matsuishi, K.; Nagasaki, Y. Multistimuli-Triggered Release of Charged Dye from Smart PEGylated Nanogels Containing Gold Nanoparticles to Regulate Fluorescence Signals. *J. Mater. Chem.* **2009,** *19*, 5909–5912.
37. Bigot, J.; Charleux, B.; Cooke, G.; Delattre, F.; Fournier, D.; Lyskawa, J.; Sambe, L.; Stoffelbach, F.; Woisel, P. Tetrathiafulvalene End-Functionalized Poly(*N*-isopropylacrylamide): A New Class of Amphiphilic Polymer for the Creation of Multistimuli Responsive Micelles. *J. Am. Chem. Soc.* **2010,** *132*, 10796–10801.
38. Deng, Y.; Wang, C.; Shen, X.; Yang, W.; Jin, L.; Gao, H.; Fu, S. Preparation, Characterization, and Application of Multistimuli-Responsive Microspheres with Fluorescence-Labeled Magnetic Cores and Thermoresponsive Shells. *Chem.—Eur. J.* **2005,** *11*, 6006–6013.
39. Foster, J. A.; Steed, J. W. Exploiting Cavities in Supramolecular Gels. *Angew. Chem., Int. Ed.* **2010,** *49*, 6718–6724.
40. Wang, Y.; Xu, H.; Zhang, X. Tuning the Amphiphilicity of Building Blocks: Controlled Self-Assembly and Disassembly for Functional Supramolecular Materials. *Adv. Mater.* **2009,** *21*, 2849–2864.
41. Kimizuka, N.; Kawasaki, T.; Kunitake, T. Self-Organization of Bilayer Membranes from Amphiphilic Networks of Complementary Hydrogen Bonds. *J. Am. Chem. Soc.* **1993,** *115*, 4387–4388.
42. Kimizuka, N.; Kawasaki, T.; Hirata, K.; Kunitake, T. Supramolecular Membranes. Spontaneous Assembly of Aqueous Bilayer Membrane *via* Formation of Hydrogen Bonded Pairs of Melamine and Cyanuric Acid Derivatives. *J. Am. Chem. Soc.* **1998,** *120*, 4094–4104.
43. Zhang, X.; Chen, Z.; Würthner, F. Morphology Control of Fluorescent Nanoaggregates by Co-Self-Assembly of Wedge- and Dumbbell-Shaped Amphiphilic Perylene Bisimides. *J. Am. Chem. Soc.* **2007,** *129*, 4886–4887.
44. Kim, K.; Jeon, W. S.; Kang, J.-K.; Lee, J. K.; Jon, S. Y.; Kim, T.; Kim, K. A Pseudorotaxane on Gold: Formation of Self-Assembled

Monolayers, Reversible Dethreading and Rethreading of the Ring, and Ion-Gating Behavior. *Angew. Chem., Int. Ed.* **2003,** *42*, 2293–2296.
45. Pisula, W.; Kastler, M.; Wasserfallen, D.; Robertson, J. W. F.; Nolde, F.; Kohl, C.; Müllen, K. Pronounced Supramolecular Order in Discotic Donor−Acceptor Mixtures. *Angew. Chem., Int. Ed.* **2006,** *45*, 819–823.
46. Wang, Y.; Ma, N.; Wang, Z.; Zhang, X. Photocontrolled Reversible Supramolecular Assemblies of an Azobenzene-Containing Surfactant with α-Cyclodextrin. *Angew. Chem., Int. Ed.* **2007,** *46*, 2823–2826.
47. Wang, C.; Yin, S.; Chen, S.; Xu, H.; Wang, Z.; Zhang, X. Controlled Self-Assembly Manipulated by Charge-Transfer Interactions: From Tubes to Vesicles. *Angew. Chem., Int. Ed.* **2008,** *47*, 9049–9052.
48. Würthner, F. Perylene Bisimide Dyes as Versatile Building Blocks for Functional Supramolecular Architectures. *Chem. Commun.* **2004,** 1564–1579.
49. Ko, Y. H.; Kim, E.; Hwang, I.; Kim, K. Supramolecular Assemblies Built with Host-Stabilized Charge-Transfer Interactions. *Chem. Commun.* **2007,** 1305–1315.
50. Wan, P.; Jiang, Y.; Wang, Y.; Wang, Z.; Zhang, X. Tuning Surface Wettability through Photocontrolled Reversible Molecular Shuttle. *Chem. Commun.* **2008,** 5710–5712.
51. Bize, C.; Garrigues, J.-C.; Blanzat, M.; Rico-Lattes, I.; Bistri, O.; Colasson, B.; Reinaud, O. Spontaneous Formation of Vesicles in a Catanionic Association Involving a Head and Tail Functionalized Amino-Calix[6]arene. *Chem. Commun.* **2010,** *46*, 586–588.
52. Jeon, Y. J.; Bharadwaj, P. K.; Choi, S. W.; Lee, J. W.; Kim, K. Supramolecular Amphiphiles: Spontaneous Formation of Vesicles Triggered by Formation of a Charge-Transfer Complex in a Host. *Angew. Chem., Int. Ed.* **2002,** *41*, 4474–4476.
53. Jing, B.; Chen, X.; Wang, X.; Yang, C.; Xie, Y.; Qiu, H. Self-Assembly Vesicles Made from a Cyclodextrin Supramolecular Complex. *Chem.—Eur. J.* **2007,** *13*, 9137–9142.
54. Zeng, J.; Shi, K.; Zhang, Y.; Sun, X.; Zhang, B. Construction and Micellization of a Noncovalent Double Hydrophilic Block Copolymer. *Chem. Commun.* **2008,** 3753–3755.
55. Guo, D.-S.; Chen, K.; Zhang, H.-Q.; Liu, Y. Nano-Supramolecular Assemblies Constructed from Water-Soluble Bis(calix-[5]arenes) with Porphyrins and Their Photoinduced Electron Transfer Properties. *Chem. Asian J.* **2009,** *4*, 436–445.
56. Perret, F.; Lazar, A. N.; Coleman, A. W. Biochemistry of the *para*-Sulfonato-Calix[*n*]arenes. *Chem. Commun.* **2006,** 2425–2438.
57. Coleman, A. W.; Jebors, S.; Cecillon, S.; Perret, P.; Garin, D.; Marti-Battle, D.; Moulin, M. Toxicity and Biodistribution of *para*-Sulfonato-Calix[4]arene in Mice. *New J. Chem.* **2008,** *32*, 780–782.
58. Wang, K.; Guo, D.-S.; Zhang, H.-Q.; Li, D.; Zheng, X.-L.; Liu, Y. Highly Effective Binding of Viologens by *p*-Sulfonatocalixarenes for the Treatment of Viologen Poisoning. *J. Med. Chem.* **2009,** *52*, 6402–6412.
59. Uzunova, V. D.; Cullinane, C.; Brix, K.; Nau, W. M.; Day, A. I. Toxicity of Cucurbit[7]uril and Cucurbit[8]uril: An Exploratory *in Vitro* and *in Vivo* Study. *Org. Biomol. Chem.* **2010,** *8*, 2037–2042.
60. Stella, V. J.; Rajewski, R. A. Cyclodextrins: Their Future in Drug Formulation and Delivery. *Pharm. Res.* **1997,** *14*, 556–567.
61. Uekama, K.; Hirayama, F.; Irie, T. Cyclodextrin Drug Carrier Systems. *Chem. Rev.* **1998,** *98*, 2045–2076.
62. Kellermann, M.; Bauer, W.; Hirsch, A.; Schade, B.; Ludwig, K.; Böttcher, C. The First Account of a Structurally Persistent Micelle. *Angew. Chem., Int. Ed.* **2004,** *43*, 2959–2962.
63. Ryu, E.-H.; Zhao, Y. Environmentally Responsive Molecular Baskets: Unimolecular Mimics of Both Micelles and Reversed Micelles. *Org. Lett.* **2004,** *6*, 3187–3189.
64. Sugiyama, K.; Esumi, K.; Koide, Y. Aqueous Properties of Resorcinol-Type Calix[4]arenes Bearing Four Alkyl Side Chains. *Langmuir* **1996,** *12*, 6006–6010.
65. Tanaka, Y.; Miyachi, M.; Kobuke, Y. Selective Vesicle Formation from Calixarenes by Self-Assembly. *Angew. Chem., Int. Ed.* **1999,** *38*, 504–506.
66. Houmadi, S.; Coquière, D.; Legrand, L.; Fauré, M. C.; Goldmann, M.; Reinaud, O.; Rémita, S. Architecture-Controlled "SMART" Calix[6]arene Self-Assemblies in Aqueous Solution. *Langmuir* **2007,** *23*, 4849–4855.
67. Micali, N.; Villari, V.; Consoli, G. M. L.; Cunsolo, F.; Geraci, C. Vesicle-to-Micelle Transition in Aqueous Solutions of Amphiphilic Calixarene Derivatives. *Phys. Rev. E* **2006,** *73*, 051904–051908.
68. Israelachvilli, J. N. *Intermolecular and Surface Forces*; Academic Press: New York, 1985.
69. Wang, K.; Guo, D.-S.; Liu, Y. Temperature-Controlled Supramolecular Vesicles Modulated by *p*-Sulfonatocalix-[5]arene with Pyrene. *Chem.—Eur. J.* **2010,** *16*, 8006–8011.
70. Francisco, V.; Basilio, N.; García-Río, L.; Leis, J. R.; Maques, E. F.; Vázquez-Vázquez, C. Novel Catanionic Vesicles from Calixarene and Single-Chain Surfactant. *Chem. Commun.* **2010,** *46*, 6551–6553.
71. Krieg, M.; Pileni, M.-P.; Braun, A. M.; Gratzel, M. Micelle Formation and Surface Activity of Functional Redox Relays: Viologens Substituted by a Long Alkyl Chain. *J. Colloid Interface Sci.* **1981,** *83*, 209–213.
72. Diaz, A.; Quintela, P. A.; Schuette, J. M.; Kaifer, A. E. Complexation of Redox-Active Surfactants by Cyclodextrins. *J. Phys. Chem.* **1988,** *92*, 3537–3542.
73. Lee, Y.; Lee, C. Electrochemical Behavior of Viologens with Long Alkyl Chains Depending on Their Concentrations and the Concentration of Micelles and Cyclodextrins. *Bull. Korean Chem. Soc.* **1999,** *20*, 1–8.
74. Menger, F. M. The Structure of Micelles. *Acc. Chem. Res.* **1979,** *12*, 111–117.
75. Rehm, M.; Frank, M.; Schatz, J. Water-Soluble Calixarenes—Self-Aggregation and Complexation of Noncharged Aromatic Guests in Buffered Aqueous Solution. *Tetrahedron Lett.* **2009,** *50*, 93–96.
76. Guo, D.-S.; Su, X.; Liu, Y. Benzyl Effects of Supramolecular Architectures Constructed by *p*-Sulfonatocalix[4]arene and Viologen Guests: From Simple 2:1 Complex to Polymeric Capsules. *Cryst. Growth Des.* **2008,** *8*, 3514–3517.
77. Jeon, W. S.; Ziganshina, A. Y.; Lee, J. W.; Ko, Y. H.; Kang, J.-K.; Lee, C.; Kim, K. A [2]Pseudorotaxane-Based Molecular Machine: Reversible Formation of a Molecular Loop Driven by Electrochemical and Photochemical Stimuli. *Angew. Chem., Int. Ed.* **2003,** *42*, 4097–4100.
78. Guo, D.-S.; Wang, K.; Liu, Y. Selective Binding Behaviors of *p*-Sulfonatocalixarenes in Aqueous Solution. *J. Inclusion Phenom. Macrocyclic Chem.* **2008,** *62*, 1–21.
79. Chen, Z.; Lohr, A.; Saha-Möller, C. R.; Würthner, F. Self-Assembled π-Stacks of Functional Dyes in Solution: Structural and Thermodynamic Features. *Chem. Soc. Rev.* **2009,** *38*, 564–584.
80. Chen, Z.; Stepanenko, V.; Dehm, V.; Prins, P.; Siebbeles, L. D. A.; Seibt, J.; Marquetand, P.; Engel, V.; Würthner, F. Photoluminescence and Conductivity of Self-Assembled π−π Stacks of Perylene Bisimide Dyes. *Chem.—Eur. J.* **2007,** *13*, 436–449.
81. Guo, D.-S.; Wang, L.-H.; Liu, Y. Highly Effective Binding of Methyl Viologen Dication and Its Radical Cation by *p*-Sulfonatocalix[4,5]arenes. *J. Org. Chem.* **2007,** *72*, 7775–7778.
82. Castro, R.; Godínez, L. A.; Criss, C. M.; Kaifer, A. E. Host Properties of α-Cyclodextrin and a Water-Soluble Calix-[6]arene Probed with Dimeric Bipyridinium Guests. *J. Org. Chem.* **1997,** *62*, 4928–4935.
83. The pH value for this C4AS + MVC_{12} system is 5.31. C4AS was employed in this system for the reason that in comparison with *p*-sulfonatocalix[5]arene and *p*-sulfonatothiacalix-[4]arene, C4AS shows the more favorable enthalpy changes upon complexation with viologen under both acidic and neutral conditions. Moreover, the larger analogue, *p*-sulfonatocalix[6]arene, was also excluded because of its uncertain conformation and relatively weak binding ability.
84. Kusumoto, Y.; Shizuka, M.; Satake, I. Absorption and Fluorescence Studies of the Interaction of Pyrene with β-Cyclodextrin in Aqueous Surfactant Solutions. *Chem. Phys. Lett.* **1986,** *125*, 64–68.

85. Jeon, W. S.; Kim, H.-J.; Lee, C.; Kim, K. Control of the Stoichiometry in Host−Guest Complexation by Redox Chemistry of Guests: Inclusion of Methylviologen in Cucurbit[8]uril. *Chem. Commun.* **2002,** 1828–1829.
86. Arena, G.; Contino, A.; Lombardo, G. G.; Sciotto, D. Water-Soluble Calix[6]arenes. Characterization of 5,11,17,23, 29,35-Hexasulphonate-37,38,39,40,41,42-Hexahydroxycalix[6]arene and Thermodynamic Study of Proton Complex Formation. *Thermochim. Acta* **1995,** *264*, 1–11.
87. Lei, Y.; Hurst, J. K. Reduction Potentials of Vesicle-Bound Viologens. *J. Phys. Chem.* **1991,** *95*, 7918–7925.
88. Matsumiya, H.; Terazono, Y.; Iki, N.; Miyano, S. Acid−Base Properties of Sulfur-Bridged Calix[4]arenes. *J. Chem. Soc., Perkin Trans. 2* **2002,** 1166–1172.